Upcycling Waste: *Citrus limon* Peel-Derived Carbon Quantum Dots for Sensitive Detection of Tetracycline in the Nanomolar Range

Aayushi Kundu, Soumen Basu,* and Banibrata Maity*

Read Online
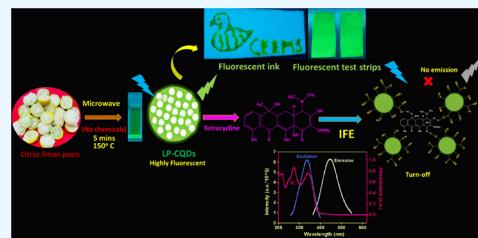
ACCESS | Metrics & More | Article Recommendations | SI Supporting Information

ABSTRACT: In this work, a sustainable method was developed for the production of water-soluble carbon quantum dots employing a green approach. The synthetic protocol was employed using the microwave pyrolysis technique, while lemon peel served as a carbon precursor. Fabrication of highly fluorescent lemon-peel-derived CQDs (LP-CQDs) having inherent nitrogen functionality was validated by X-ray photoelectron spectroscopy, FTIR, X-ray diffraction, Raman spectroscopic analysis, and TEM techniques. The average particle size of fabricated LP-CQDs was 4.46 nm. LP-CQDs yielded a remarkable quantum yield of 49.5%, which displayed excellent salinity, photostability, storage time, conditions, and pH stability. LP-CQDs displayed encouraging results for tetracycline (TC) detection using a PL turn-off approach. The sensitivity of LP-CQDs toward TC was seen in a nanomolar range having a detection limit of 50.4 nM. Method validation was comprehensively studied to ensure the precision of the nanosensor. A complete analysis of different photophysical parameters of LP-CQDs was performed with TC to gain a deeper understanding of the sensing mechanism. Fabricated LP-CQDs showed fluorescence quenching toward TC, elucidated by the inner filter effect (IFE) mechanism. The synthesized nanoprobe demonstrated a lesser detection limit with a broad linear range, enabling facile, cheap, environmentally friendly, and fast detection of TC. Practicality of the detection method was assessed through analysis of real samples, resulting in satisfactory recovery percentage and relative standard deviation with respect to the developed probes. Furthermore, LP-CQDs were used as fluorescent inks and to fabricate paper-based fluorescent strips. This study lays the door for the sensing platform of LP-CQDs toward detection of TC, which may impact the potential role of environmental sustainability.

INTRODUCTION

The emerging science of nanotechnology has substantial influence on a number of disciplines, including chemistry, optics, medicine, thermology, and electricity. Recently, nano-materials research has captivated the interest of scientists and engineers worldwide.[1] Carbon dots have garnered considerable attention as unique fluorescent zero-dimensional nanomaterial. Carbon quantum dots (CQDs) have an average diameter of less than 10 nm and a spherical shape, with carbon networks arranged by sp^2- and sp^3-hybridized carbon atoms.[2] CQDs are regarded as excellent nanoprobes for a variety of applications in optoelectronics, sensors, biomedicines, drug administrations, catalysis, and biological imaging, due to their outstanding photostability, highly tunable photoluminescence (PL) property, water solubility, compact size, low toxicity, favorable biocompatibility, electrochemiluminescence capability, and eco-friendly nature.[3]

Generally, CQDs have been synthesized using organic compounds and naturally available precursors, including biomass. Organic chemicals like glycerol, chitosan, and citric acid have been used for developing CQDs, but they have certain limitations such as harsh reaction conditions, requirements for postsurface passivation/modification, high cost, and toxicity.[4,5] Therefore, it is desirable to use affordable, facile, and ecologically benign methods to synthesize CQDs using biomass waste as a
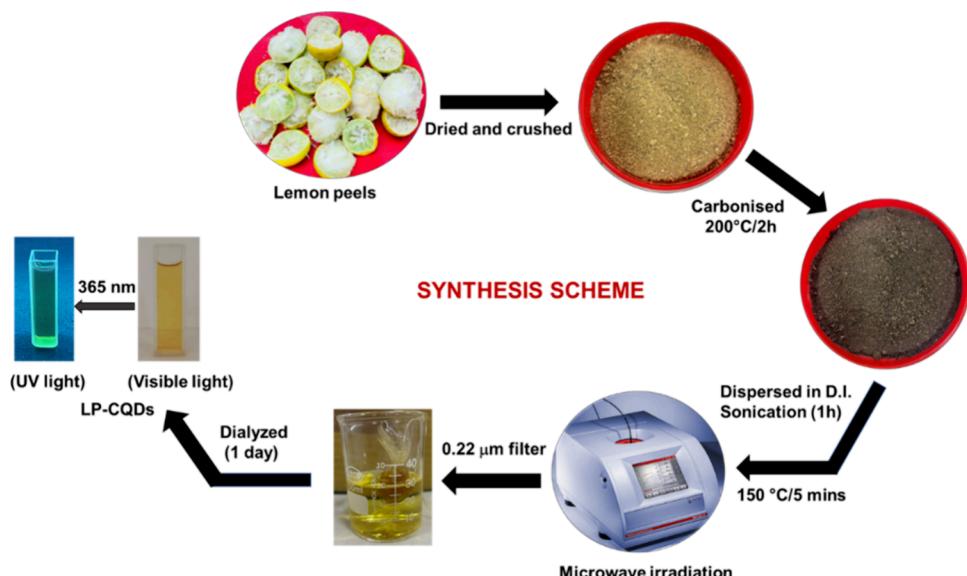
precursor. Also, transforming biomass into high-value products serves a dual purpose: effectively managing solid waste disposal and alleviating escalating resource, environmental, and energy challenges. Natural biomass inherently possesses a substantial amount of oxygen, carbon, and heteroatoms such as nitrogen (N) and sulfur (S), which impart self-passivation or self-doping properties to CQDs. The abundant presence of various functional oxygenic groups like hydroxyl, alkyl, epoxide, carboxyl, and carbonyl on the biomass-derived CQD surface contributes to their remarkable water-soluble characteristics.[6] *Citrus limon*, commonly known as lemon, is the most significant citrus fruit in the world, serving both culinary and nonculinary purposes.[7] However, once the juice is extracted, the peels are frequently discarded away and allowed to biodegrade, which potentially pollutes air by forming dust.[8] Therefore, it is essential to research low-cost strategies for transforming lemon peel into value-added products. Remarkably, the lemon peels are rich in

Scheme 1. Fabrication of LP-CQDs from *Citrus limon* Peels

proteins and fibers, which can serve as a potential carbon source for synthesizing CQDs. Tyagi et al. synthesized CQDs using lemon peel via a hydrothermal method with a quantum yield of 14%. They used synthesized CQDs for the detection of Cr^{6+}.[8] Su et al. fabricated CQDs from dried lemon peels through the hydrothermal method with 11% quantum yield for the detection of carmine.[9] Vadia et al. used lemon peels for the synthesis of carbon dots for the detection of Fe^{3+} and propiconazole pesticide using a turn off–on mechanism with a quantum yield of 32%. However, the limitation found in the literature of lemon peel-derived CQDs is achieving high quantum yield.

Tetracycline (TC), a broad-spectrum antibiotic with excellent sterilization, disinfection efficiency, antimicrobial activity, and low toxicity, is a cost-effective option. It is extensively utilized in animal husbandry to effectively combat various bacteria that cause diseases including rickettsia, chlamydia, and mycoplasma.[10] However, improper use of TC in veterinary medication along with food products has led to its presence in common food such as milk, meat, and honey.[11] This causes a major risk to human health including liver damage, visual problems, bacterial resistance, and human tooth problems.[12] Due to these side effects, numerous analytical techniques, including enzyme-linked immunosorbent assays,[13] capillary electrophoresis,[14] electrochemical studies,[15] high-performance liquid chromatography (HPLC),[16] and other various techniques have been developed to identify TC antibiotics. Nevertheless, these techniques necessitate time-consuming sample preparation stages, costly equipment, and professional operators, becoming considerable hurdles for real detection.

To overcome these disadvantages, a fluorescence-based technique has gained attention as a viable alternative for the quantification and detection of TCs. These methods offer operational convenience, affordability, real-time detection capabilities, high sensitivity and selectivity, and fast analysis time.[2,3,17,18] Liu et al. synthesized blue emissive europium-doped CQDs using carbonization, using them for TC detection with a 0.3 μM limit of detection.[19] Fan et al. fabricated S, N-doped CQDs for the detection of TC antibiotics with a 0.56 μmol/L detection limit in the range of 1.88−60 μmol/L.[20] Wang et al. prepared N-CQDs with a quantum yield of 10.97% from ethylenediamine and glucose for the detection of TC
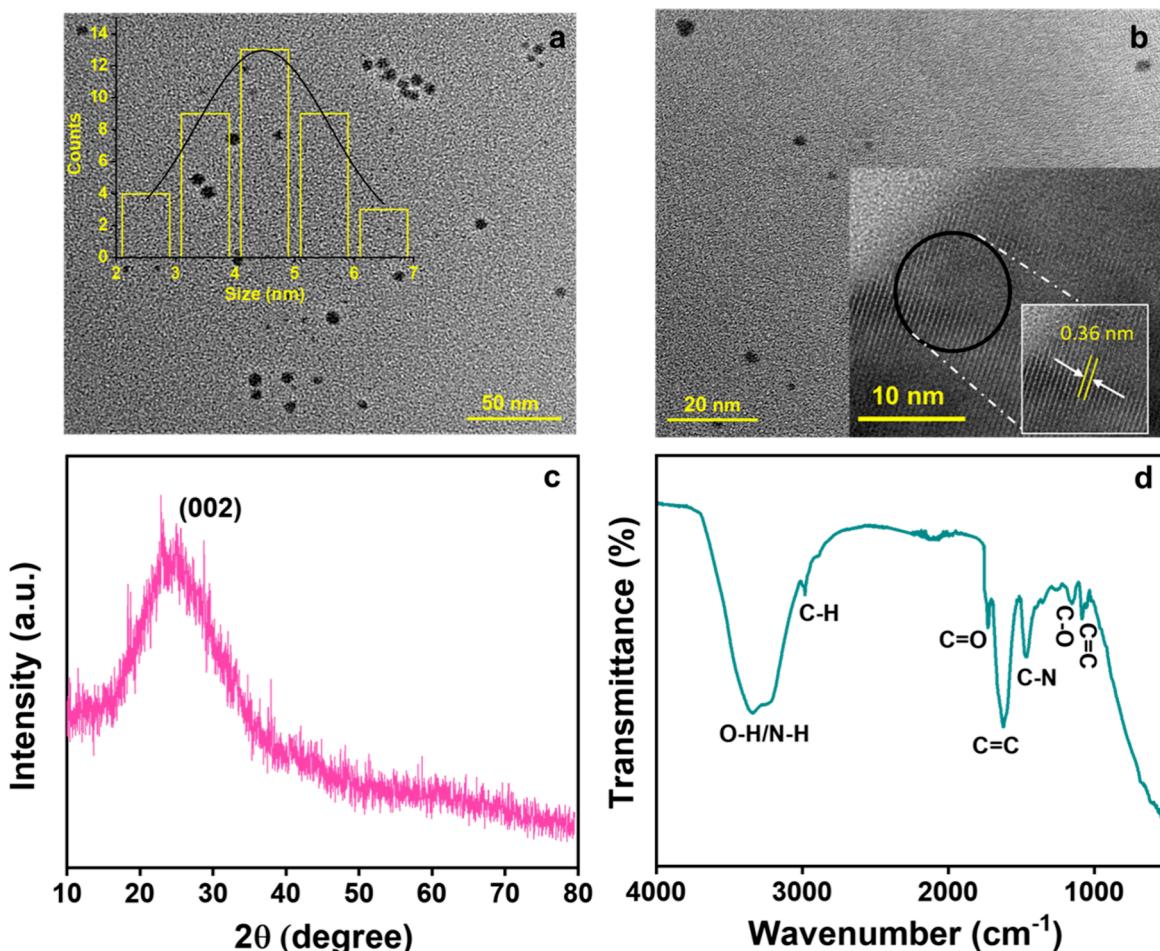
antibiotics such as chlortetracycline, oxytetracycline, and TC with 0.117, 0.265, and 0.344 μM, respectively.[11] Qi et al. utilized rice residue and glycine as biomass precursors for fabrication of N-doped CQDs using the hydrothermal method, which was used for the detection of Fe^{3+} and TC.[21] Zhang and Fan fabricated Ce−N-codoped CQDs with low cytotoxicity for TC residues and bioimaging with the detection limit of 0.25 μM.[22] John et al. utilized *Ruta graveolens* leaves for the preparation of CQDs with an 18% quantum yield. The probe was used for the electrochemical sensing of TC.[23]

In this paper, biomass-derived CQDs were synthesized as a fluorescent nanoprobe from dried peels of *C. limon*, abbreviated as LP-CQDs. The synthesis methodology was purely maintained in green protocol without the usage of any chemicals with high quantum yield (49.5%). The fluorescent nanoprobe with inherent nitrogen was sustainable, simple, and inexpensive. The formation of LP-CQDs was stable and displayed excellent selectivity toward TC. Therefore, it was utilized as an efficacious probe for quantitative detection of TC in real samples of river, tap water, and tablet. The outcome of the present study possesses special aspects and offers many advantages compared to earlier literature studies: (i) The synthesis of LP-CQDs utilizes a readily available and eco-friendly biowaste with reduced time requirement; (ii) the synthesis was done without the incorporation of any harsh chemicals and complex techniques; (iii) high quantum yield was observed with nanomolar-level detection of TC; and (iv) the sensor is free from metallic components, enabling its safe application across various fields without any adverse effects.

■ MATERIALS AND METHODS

Lemon peels were taken from a local juice shop in Patiala, India. Tetracycline hydrochloride was procured from Sigma-Aldrich and used as such. Dialysis Membrane-110 was acquired from HiMedia Laboratories Private Limited. The chemicals essential to making solutions of metal ions and other analytes were bought from Loba Chemie. Deionized (D.I.) water was used for experiments.

Synthesis of Lemon Peel-Carbon Quantum Dots (LP-CQDs). First, lemon peels were thoroughly cleaned with D.I.

Figure 1. (a) TEM image of LP-CQDs with the inset representing the size distribution histogram. (b) TEM image with the inset showing lattice spacing. (c) XRD spectrum and (d) FTIR spectrum of LP-CQDs.

water and oven-dried at 90 °C, followed by grinding in a mixer. The powder was carbonized at 200 °C for 2 h in a muffle furnace. The collected black powder was dispersed in D.I. water, sonicated for 1 h, and transferred to a vial, which was retained for heating for 5 min at 150 °C (300 W) under microwave irradiation. Collected solution was filtered with a 0.22 μm syringe filter and then kept in a dialysis bag (1 day) to obtain light-brown-colored LP-CQDs (Scheme 1).

Sample-Solution Formulation. Standard solutions (1 mM) of different metal cations (Co^{2+}, Fe^{3+}, Zn^{2+}, Al^{3+}, Cr^{3+}, Cu^{2+}, Ni^{2+}, Hg^{2+}, Fe^{2+}) and analytes (amoxicillin (AC), ofloxacin (OFX), ascorbic acid (AA), ciprofloxacin (CPX), TC, nitrobenzene (NB), levofloxacin (LF), streptomycin (SPM), chlortetracycline (CTC), and thiamethoxam (TM)) were prepared in D.I. water for the selectivity experiments of prepared LP-CQDs. 20 μL of LP-CQDs in 2 mL of D.I. water along with 0.1 mM of the analyte solution was pipetted in a cuvette, and emission spectra were measured. The sensitivity was studied using stock solution of 1 μM of TC.

Real-Sample Analysis. To inspect the utility of the developed sensing system, the study was carried out with real samples (river water and tap water). The water sample was collected from the Bhakra River in Patiala. The collected samples were subjected to filtration using nylon filters before the analysis using nylon filters having a pore size of 0.45 μm. Following the addition of specific concentrations of TC

(spiking) to the samples, LP-CQDs were added. The fluorescence studies were carried out at 330 nm.
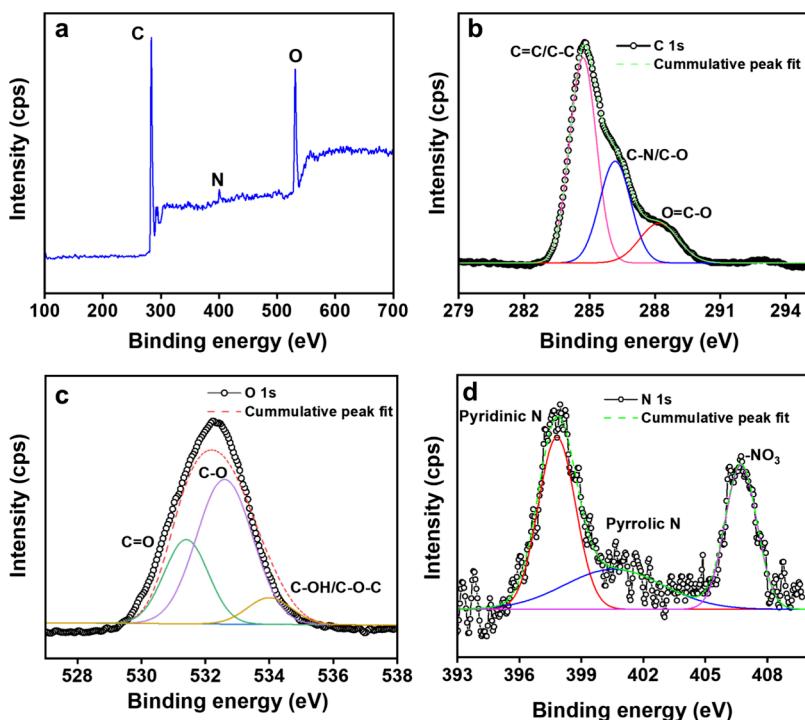
Measurement of Quantum Yield. Quantum yield (QY) is vital for analyzing properties of fluorescent materials. The QY of LP-CQDs in the presence of TC was recorded with quinine sulfate[24] solution as reference (ϕ_R= 0.546) using eq 1:

$$\phi_S = \phi_R \times \frac{A_S}{A_R} \times \frac{(Abs)_R}{(Abs)_S} \times \frac{\eta_S^2}{\eta_R^2} \tag{1}$$
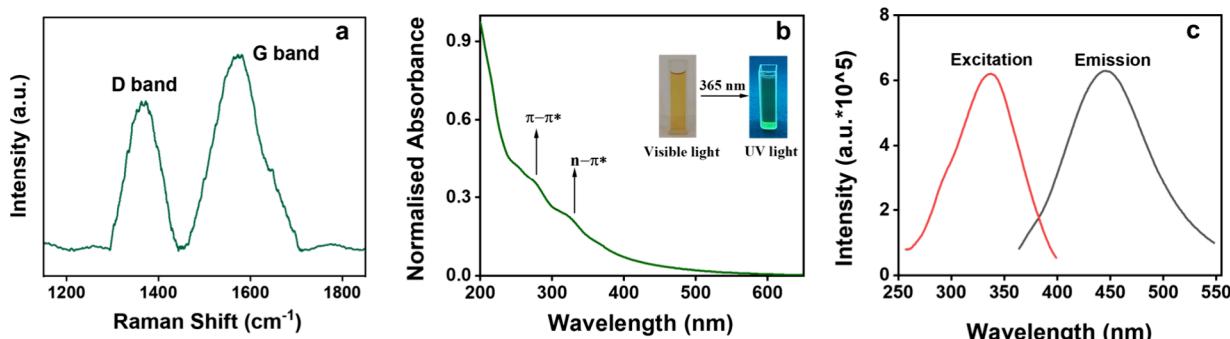
"ϕ_s" and "ϕ_R" denote the QY of LP-CQDs and quinine sulfate, respectively. "η", "Abs", and "A" refer to the refractive index, absorbance, and integral area of PL emission, respectively. The subscripts "R" and "S" represent reference and sample, respectively.

■ RESULTS AND DISCUSSION

Characterizations. TEM was used to examine the morphology and size of the fabricated LP-CQDs. Figure 1a,b displays the nearly spherical particles with monodispersity. The inset of Figure 1a illustrates the particle size histogram ranging from 2 to 7 nm, having a particle size of 4.46 nm. Lattice fringes of 0.36 nm resemble the (002) graphitic plane (Figure 1b inset).[25] The hydrodynamic particle size was calculated to be ~52 nm using DLS data (Supporting Figure S1a). Figure 1c depicts the XRD of LP-CQDs with a diffraction peak at 2θ = 24.5° indexing to the C(002) plane.[25] The d-spacing was

Figure 2. (a) Survey graph of LP-CQDs. High-resolution spectra of (b) C 1s, (c) O 1s, and (d) N 1s of LP-CQDs.

Figure 3. (a) Raman spectrum of LP-CQDs, and (b) UV−vis. absorption spectra with inset showing LP-CQDs in UV and Visible light, and (c) excitation and emission spectra of LP-CQDs.
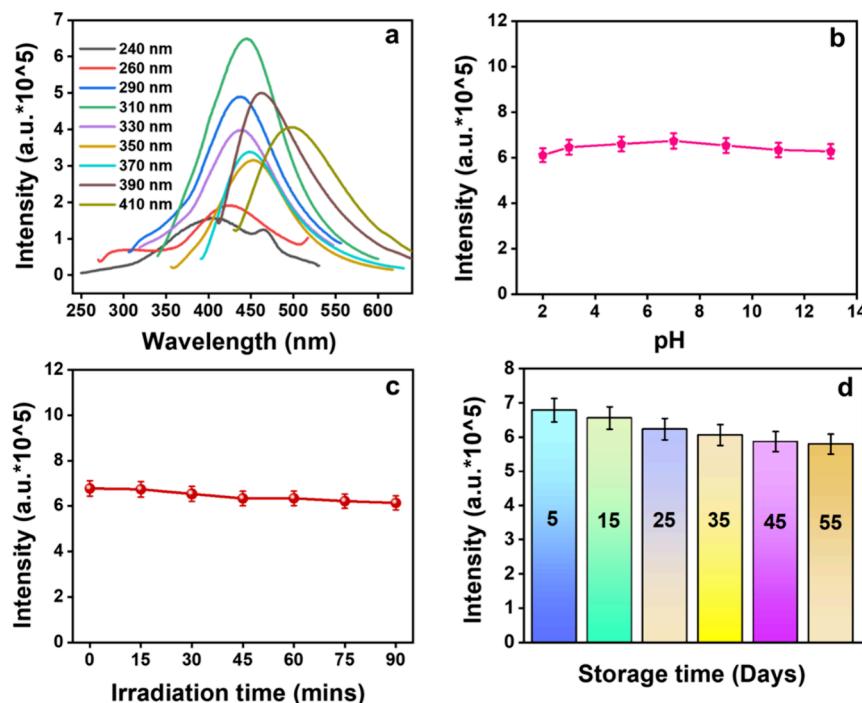
determined by using Bragg's equation ($n\lambda = 2d\sin\theta$), which is consistent with the HR-TEM results. The FTIR spectra in Figure 1d show a broad peak at 3200−3400 cm^{-1}, which corresponds to the O−H/N−H stretching vibrations. A minor band appears at 2976 cm^{-1} signifying C−H stretching vibration, and signals at 1732 and 1626 cm^{-1} are attributed to C═O and C═C stretching vibrations, respectively. Signals at 1467 cm^{-1} resemble C−N stretching. Peaks at 1266 and 1159 cm^{-1} confirm the C−O stretching. The peak at 1088 cm^{-1} is attributed to C═C bending vibrations.[26] The occurrence of the hydrophilic functionalities on LP-CQDs, as obtained from FTIR analysis, signifies the reason for excellent water solubility.[23] The zeta potential was −17. 5 mV affirms the abundance of negatively charged functional groups on LP-CQDs (Figure S1b).[27]

An XPS analysis was conducted to determine the surface composition and oxidation states of LP-CQDs. The survey spectrum in Figure 2a shows the peaks at 284.5, 400.1, and 532.2 eV allocated to C (78.96%), N (5.67%), and O (15.37%), respectively.[28] C 1s (Figure 2b) high-resolution spectra showed three peaks at 284.7, 286.2, and 288.2 eV ascribed to C−C/C═ C, C−O/C−N, and C═O/C═N groups, respectively. O 1s
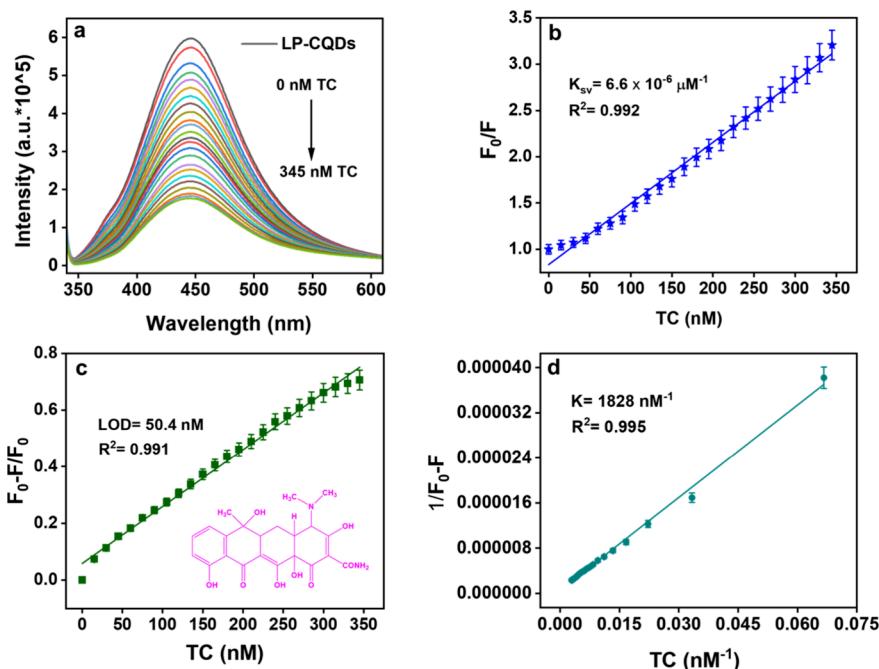
spectra exhibited peaks at 531.3, 532.6, and 534.0 eV conforming to C═O, C−O, and C−OH/C−O−C, respectively (Figure 2c).[23] N 1s spectra (Figure 2d) showed peaks at 397.8 and 400.3 eV corresponding to pyridinic and pyrrolic N, respectively,[29] while a strong peak was seen at 406.8, which is due to existence of −NO$_3$.[30] The occurrence of these functional groups indicates the hydrophilicity on the LP-CQD surface, which aligns with FTIR results.

Raman spectra (Figure 3a) of LP-CQDs displayed two broad peaks at 1368 and 1574 cm^{-1} representing D (sp^3-hybridized disordered D) and G (sp^2-hybridized graphitic G) bands, respectively, with an I_D/I_G band intensity of 0.86.[23] The observed I_D/I_G ratio is less than 1, signifying the well-graphitized carbon components.[23] Raman results confirmed the existence of both sp^2 carbon (G) with defective sp^3 carbons (D) within LP-CQDs.[3]

Optical Studies of LP-CQDs. UV−vis absorption spectra were employed, in conjunction with fluorescence emission spectra, to investigate the optical properties. Figure 3b shows a shoulder band at around 272 and 320 nm, which are assigned to $\pi-\pi^*$ transitions of sp^2 C═C bonds and $n-\pi^*$ transitions of

Figure 4. (a) PL emission spectra of LP-CQDs under various excitation wavelengths, (b) The influence of pH (2−13) on PL emission behavior of LP-CQDs, (c) impact of irradiation time (in min), and (d) Effect of storage time (in days) on the fluorescence emission of LP-CQDs.

Figure 5. (a) Change in fluorescence intensity of LP-CQDs with the change in concentrations of TC. (b) Stern−Volmer plot of LP-CQDs. (c) Linear relation between fluorescence response ($F_0 - F/F_0$) and different concentrations of TC with the inset image showing the TC structure. (d) B−H plot of TC with LP-CQDs.

C=O of LP-CQDs.[31] The LP-CQDs emit a strong emissive green fluorescence upon UV-light irradiation (365 nm), while light-brown fluorescence under visible light is seen, as depicted in the inset of Figure 3b. This fluorescence emission of LP-CQDs is believed to be a result of radiative recombination between holes and electrons, which occurs due to photoinduced charge separation and surface site trapping.[32] By employing eq 1, the fluorescence QY of LP-CQDs was 49.5%. For studying

fluorescence behavior, the excitation and emission spectra were recorded, as illustrated in Figure 3c. Upon excitation of 330 nm, LP-CQDs showed the maximum PL emission intensity at 445 nm.

The fluorescence emission spectra at different excitation wavelengths were studied, as shown in Figure 4a. A bathochromic shift was observed in the emission wavelengths from 400 to 498 nm upon changing λ_{ex}. The excitation-dependent

emission observed in LP-CQDs can be attributed to factors such as the quantum confinement effect, presence of sp^2 aromatic domains, surface edge defects, and variations in size. These factors influence the fluorescence excitation energy.[33]

Stability Studies. Assessing the stability of LP-CQDs is a crucial factor to consider before proceeding with further sensing applications. Influence of pH, storage days, irradiation time, temperature, and storage conditions was studied on the PL intensity of LP-CQDs. Figure 4b shows the slight increase in PL intensity as pH varied from 2 to 7, while a small decrease in PL intensity is seen as the pH value shifts toward 13. Variation in PL intensity of LP-CQDs occurred as a result of protonation and deprotonation of emissive sites on the CQD surface.[18,34] The maximum fluorescence intensity was seen at neutral pH, and further studies were performed at pH 7 of LP-CQDs. To evaluate the photostability, LP-CQDs were irradiated with a Xe-arc lamp up to 90 min and no noticeable change in intensity was observed (Figure 4c). Additionally, LP-CQDs were subjected to a storage period of 55 days and PL spectra were periodically measured. These PL emission spectra showed minimal change in intensity throughout the duration (Figure 4d). These studies confirm the remarkable stability of LP-CQDs. The temperature dependence (20−70 °C) of the fluorescence spectrum of LP-CQDs at 330 nm excitation is shown in Figure S2a. The PL intensity of the synthesized LP-CQDs decreases with increase in temperature as the stability of the complex decreases.[35] This may be attributed to the fact that the nonradiative decay rate increases with the temperature increase, which led to a decrease in quantum efficiency along with the PL intensity.[36] Also, synthesized LP-CQDs were stored at room temperature (20 °C) and in a refrigerator (3 °C) to check the fluorescence stability and no significant difference in intensity was seen, confirming the stability of LP-CQDs (Figure S2b).

Method Validation. The method developed was validated following the guidelines specified in ICHQ2(R1) to ensure its reliability and accuracy.[37]

Linearity and Range. In order to assess the sensitivity of the prepared sensor, the effect of different concentrations of TC (nM) on the PL intensity of LP-CQDs was examined. Figure 5a illustrates the gradual quenching of fluorescence intensity of LP-CQDs when exposed to different concentrations of TC. The quenching efficiency was evaluated by plotting the graph of F_0/F vs quencher $[Q]$ concentration, following the principles of the Stern−Volmer equation.[38]

$$\frac{F_0}{F} = 1 + K_{SV}[Q] \tag{2}$$

K_{SV} signifies the Stern−Volmer quenching constant, F_0 represents the PL intensity of LP-CQDs without quencher (i.e., TC), and F is the intensity with TC. Figure 5b illustrates a linear correlation among values of F_0/F and the concentrations of TC ranging from 0 to 345 nM through a linear regression equation:

$$F_0/F = 0.0066[TC] + 0.835 \ (R^2 = 0.992) \tag{3}$$

The values of the correlation coefficient (R^2) approaching unity in Table 1 indicate the satisfactory linearity of the system.

Limit of Detection (LOD) and Quantification (LOQ). The detection limit for TC can be computed using $3\sigma/K$, while the limit of quantification is computed using $10\sigma/K$ (Table 1), where σ denotes standard deviation (intercept) and K signifies the slope of the linear line. The detection limit calculated from Figure 5c was 50.4 nM (Table 1). The LOQ value was 168.1 nM.

Table 1. Methodical Sensing Performance of the Developed Sensor for TC

parameters	TC
linearity range (nM)	0−345
limit of detection[a] (nM)	50.4
limit of quantification[b] (nM)	168.1
regression equation	$F_0/F = 0.0066$ [TC] + 0.835
correlation coefficient	0.992
binding efficacy (nM^{-1})	1828

[a]LOD = $3\sigma/K$. [b]LOQ = $10\sigma/K$; σ denotes the intercept's standard deviation, and K is the slope.

Table 2 demonstrates that the fabricated sensor demonstrates high sensitivity toward TC and boasts a lower detection limit when compared to other sensor systems documented in literature.

Table 2. Comparison of Quantum-Dot-Based Sensing Systems for TC Detection

sr. no.	sensor's system	linear range	detection limit	ref.
1	N-CQDs	0−100 μM	0.344 μM	11
2	CDs	10−400 μM	6.0 μM	39
3	self-N-doped CQDs	0.158−40 μM	158 nM	40
4	CQDs	1.0−60 μmol·L^{-1}	0.17 μmol·L^{-1}	41
5	N-GQDs	0−60 μM	0.21 μmol·L^{-1}	42
6	S, N-CDs	0−60 μM	0.25 μM	43
7	S, N-CQDs	1.88−60 μmol·L^{-1}	0.56 μmol·L^{-1}	20
8	N-CQDs	0−600 nM	60 nM	23
9	LP-CQDs	0−345 nM	50.4 nM	present work
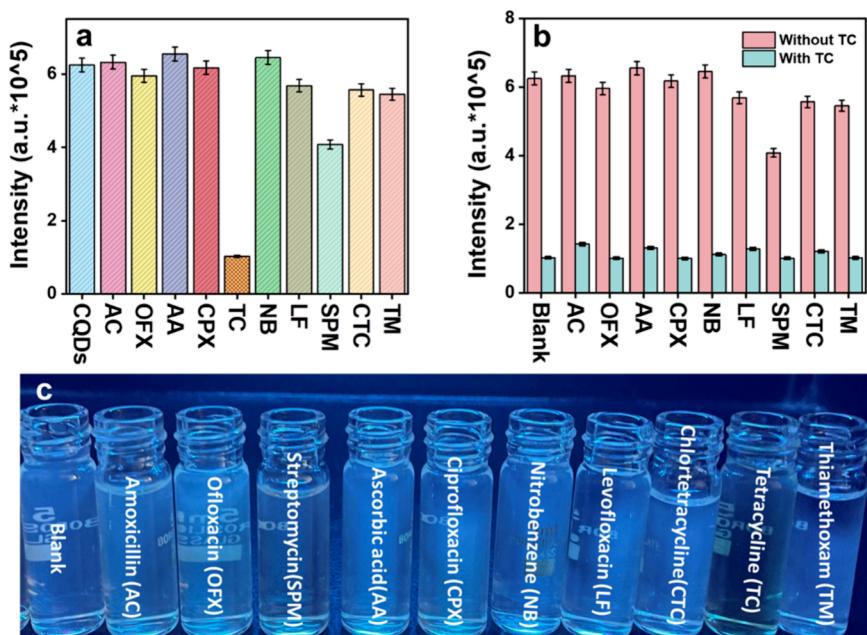
Binding Efficiency. A 1:1 linear Benesi−Hildebrand (B−H) equation was used to predict the excited-state binding constant in order to assess the binding interaction among LP-CQDs and TC.

$$\frac{1}{F_0 - F} = \frac{1}{F_0 - F_1} + \frac{1}{K[Q](F_0 - F)} \tag{4}$$
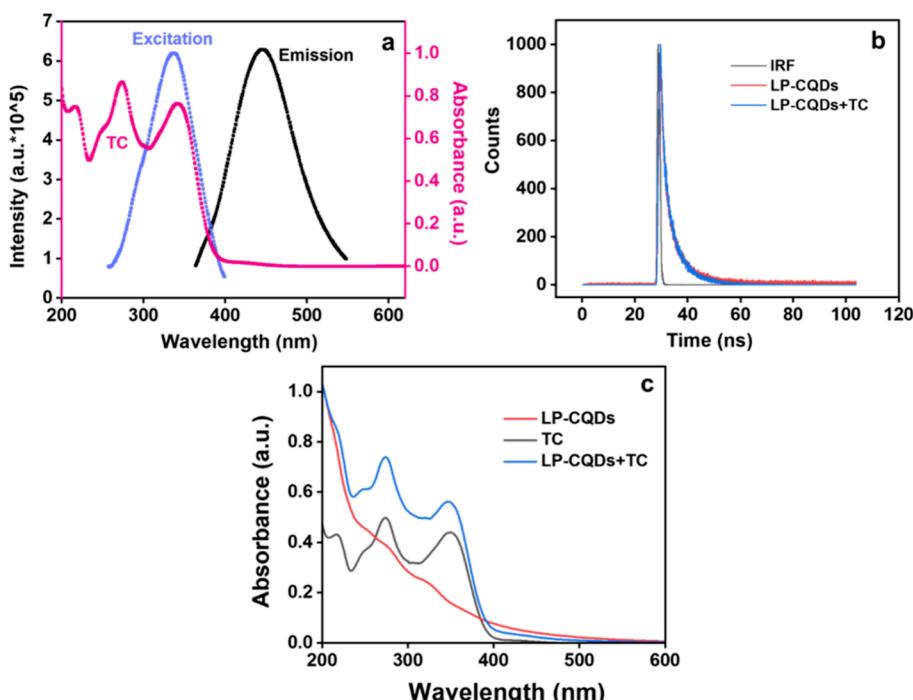
F_0 and F signify PL intensities in the absence and presence of a quencher, i.e., TC. Q signifies the quencher's concentration. F_1 is the intensity of 1:1 stoichiometric CQDs-TC. K represents the binding constant of CQDs with TC. The graph among $(1/F_0 - F)$ versus $1/[Q]$ shows a linear line with $K = 1828$ nM^{-1} and $R^2 = 0.995$ (Figure 5d, Table 1).

Precision Analysis. Three different concentrations and three replicas of each concentration were used in an experiment to determine the intraday and interday precisions. The %RSD value, which was below 2%, indicates that the method exhibits acceptable precision (Table S1).

Sensing of TC by LP-CQDs. While developing a potent sensor, it is crucial to thoroughly investigate the parameter of selectivity. The variation in the PL intensity of the LP-CQDs with 200 μL of the stock solution (1 mM) with different analytes was examined. It is clearly observed from Figure 6a that the maximum fluorescence intensity of LP-CQDs got reduced in the presence of TC. However, streptomycin (SPM) showed some quenching in intensity of LP-CQDs possibly due to hydrogen bond formation with surface groups of LP-CQDs but very less as compared to TC.[44] Fe^{3+} showed little quenching with LP-CQDs, which may be due to coordination complex formation

Figure 6. (a) Selectivity studies of LP-CQDs toward different analytes. (b) Interreference study with and without TC with diverse analytes. (c) Selectivity picture of LP-CQDs containing different analytes in UV-light irradiation.

Figure 7. (a) Overlapping of absorption spectra of TC with excitation spectra of LP-CQDs. (b) Lifetime decay curves of LP-CQDs and LP-CQDs+ TC. (c) UV−vis absorption spectra of LP-CQDs, TC, and LP-CQDs + TC.

(Figure S3).[45] Nevertheless, as shown by the interference investigations, none of these compounds significantly interfered with the detection of TC (Figure 6b). The selectivity was also studied under UV-light illumination, and it was seen that LP-CQDs have high selectivity for TC (Figure 6c). The reason for the high selectivity toward TC can be attributed to the fact that TC reacts with carboxyl and hydroxyl groups present on the LP-CQD surface, leading to quenching.[31]
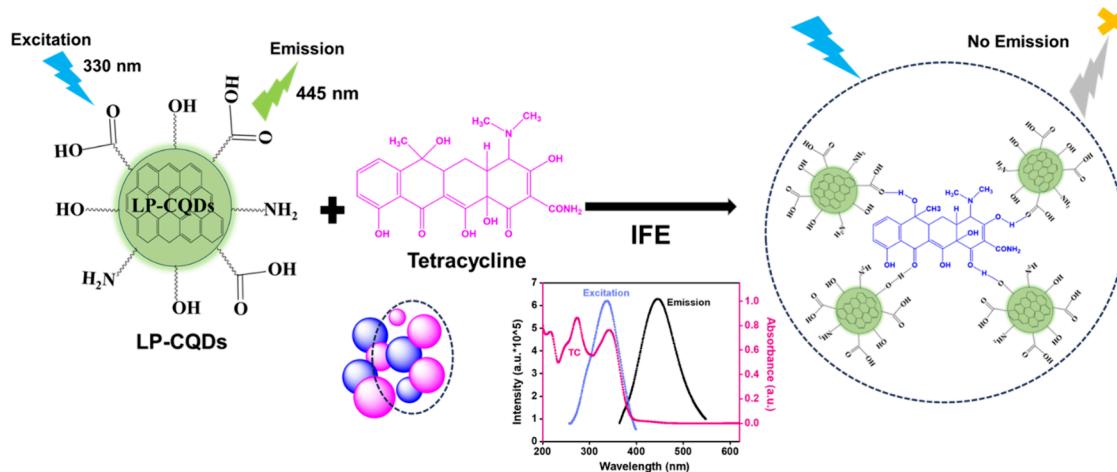
Under optimal conditions, a range of TC concentrations (0–345 nM) were added to determine the linear dynamic range and

sensitivity of LP-CQDs toward TC. As shown in Figure 5a, the intensity of LP-CQDs gradually decreased with an incremental rise in TC concentrations. Figure 5b shows the linear response of F_0/F with TC concentrations by the regression equation (F_0/F = 0.0066 [TC] + 0.835) having a 0.992 correlation coefficient. The detection limit was calculated to be 50.4 nM (Figure 5c) within the linear range 0−345 nM, which is significantly lower than the sensitivity parameters reported in earlier studies (Table 2). The LOQ was calculated to be 168.1 nM. The binding efficiency plot between ($1/F_0 - F$) vs $1/[Q]$ shows a linear line

Table 3. Fluorescence Lifetime Parameters of LP-CQDs in the Presence of TC

system	τ_1 (ns)	a_1	τ_2 (ns)	a_2	τ_3 (ns)	a_3	$^a<\tau_{av}>$ (ns)	χ^2
LP-CQDs	2.92	0.32	5.61	0.15	0.62	0.53	2.09	0.94
LP-CQDs + TC	1.97	0.28	5.89	0.22	0.38	0.50	2.03	0.93

$^a<\tau_{av}>$ (ns) $= \tau_1 a_1 + \tau_2 a_2 + \tau_3 a_3$.

Scheme 2. Plausible Mechanism of TC Detection

with $K = 1828$ nM^{-1}, $R^2 = 0.995$ (Figure 5d). Based on the results, the developed sensor offers rapid and facile detection of TC.

Quenching Mechanism. The fluorescence intensity of LP-CQDs got quenched (76.1%) in the presence of TC. The underlying process of the plausible quenching mechanism was investigated through a number of experiments. Commonly, fluorescence quenching can be attributed to five main mechanisms, namely, the inner filter effect (IFE), dynamic quenching, static quenching, photoinduced electron transfer (PET), and Forster energy resonance transfer (FRET).[46] First, optical properties of LP-CQDs and TC were studied to investigate the possibility of IFE. Figure 7a exhibits the excitation and emission spectra of LP-CQDs along with the absorption spectra of TC. Here, the TC had strong absorption peaks at 274 and 341 nm, which overlap with the excitation spectra of LP-CQDs. The phenomenon referred to as the IFE occurs when there is an overlap between the absorption band of the absorber with the excitation/emission band of the fluorophore.[47] Hence, the fluorescence quenching is attributed to the IFE. As a result, TCs would absorb the probe's excitation light, lowering its fluorescence intensity without affecting its lifetime.[48] Moreover, fluorescence studies of LP-CQDs with and without TC were performed to validate the quenching mechanism. The average lifetime values of LP-CQDs were 2.09 and 2.03 ns with the addition of TC, showing minimal change in the values of average lifetime (Figure 7b, Table 3), which signifies negligible electron transfer between LP-CQDs and TC; thus, the mechanism was attributed to the IFE.[49,50] Furthermore, the mechanism was confirmed by the UV−vis spectra of LP-CQDs, TC, and LP-CQDs + TC. Figure 7c shows the strengthening of the absorption peak in the presence of TC with no change in peak positions, signifying that no new substance was formed from LP-CQDs and TC.[10] Scheme 2 shows the plausible detection mechanism.

Real-Sample Analysis. To study the feasibility of the developed method, the detection of TC in real samples was
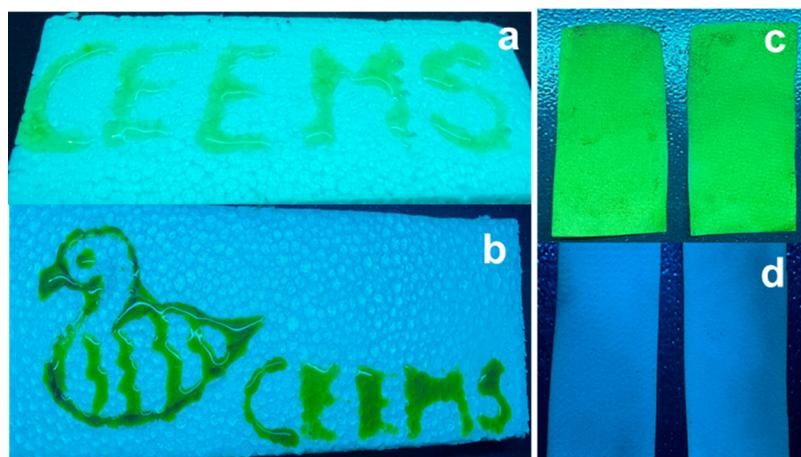
done. River water was collected from Bhakra River (Patiala), tap water was taken from Patiala, and TC tablet (Abbott) was purchased from a local market. The standard addition method was followed for the analysis. Table 4 represents the workability

Table 4. Application of the Fabricated Sensor for TC Detection in Real Samples ($n = 3$)

sample	spiked (μM)	found (μM)	recovery (%)	RSD (%)
river water	0.5	0.48	96.60	1.26
	1	1.02	102	1.29
	1.5	1.48	98.66	1.78
tap water	0.5	0.51	102.6	1.12
	1	1.02	101.9	1.52
	1.5	1.47	98.0	1.40
TC supplement	0.5	0.47	94.80	1.46
	1	1.03	103	1.47
	1.5	1.49	99.53	1.39

of LP-CQDs toward sensing of TC in river water, tap water, and tablet dosage. The data indicated a favorable percentage of recovery and a relative standard deviation (%RSD). The measured values demonstrated satisfactory precision, affirming the suitability of the prepared LP-CQDs for effective detection of TC in real samples.

Application of the Synthesized LP-CQDs as Fluorescent Ink. The green synthesis of LP-CQDs from *C. limon* peels exhibits intrinsic fluorescence and excellent aqueous stability, indicating potential for utilization in paper-based devices and fluorescent ink. The solution of LP-CQDs was used to write the fluorescent characters (handwritten words and images), as shown in Figure 8a,b, without the requirement of any sample pretreatment. Also, a paper-based fluorescence strip was made using Whatman filter paper. It shows highly green luminescence under UV-light irradiation (Figure 8c). The disappearance of green fluorescence was seen in the presence of TC (Figure 8d) making it more reliable.

Figure 8. Photographs of LP-CQDs in fluorescent characters of handwritten (a) words and (b) images. (c) Paper-based fluorescent strip of LP-CQDs and (d) LP-CQDs in the presence of TC.

CONCLUSIONS

The present study employed a cost-efficacious and environmentally friendly method to produce highly water-soluble fluorescent CQDs from lemon peel. Microwave irradiation was used without the addition of chemical substituents in the synthesis process. Intrinsic nitrogen-functionalized CQDs have been obtained without the use of any dopants. The prepared LP-CQDs are stable and emit green luminescence exhibiting excitation-dependent emission ranging from 240 to 410 nm. LP-CQDs act as a nanosensor for the highly sensitive and selective detection of TC with 76.1% quenching with a 50.4 nM detection limit in the concentration range of 0−345 nM. The fluorescence quenching was accredited to the IFE. Validation of the prepared sensor was conducted following the recommendations outlined by ICH. Furthermore, the developed method was successfully employed to detect TC in real samples, demonstrating acceptable precision and %RSD values. Also, LP-CQDs were utilized as fluorescent inks for drawing and writing without any chemical alteration. It was further successfully used to make a paper-based fluorescence strip. The present method and detection strategy offer an affordable, convenient, and sustainable approach for the detection of TC in diverse applications.

ASSOCIATED CONTENT

Supporting Information

The Supporting Information is available free of charge at https://pubs.acs.org/doi/10.1021/acsomega.3c05424.

Characterizations; precision data for detection of TC by the fabricated sensor; DLS size distribution; zeta potential of LP-CQDs; effect of temperature and storage conditions on the fluorescence stability of LP-CQDs; and selectivity of LP-CQDs with different metal ions (PDF)

AUTHOR INFORMATION

Corresponding Authors

Soumen Basu − *School of Chemistry and Biochemistry, Affiliate Faculty—TIET-Virginia Tech Center of Excellence in Emerging Materials, Thapar Institute of Engineering and Technology, Patiala 147004, India;* ⊙ orcid.org/0000-0001-6419-1326; Email: soumen.basu@thapar.edu

Banibrata Maity − *School of Chemistry and Biochemistry, Affiliate Faculty—TIET-Virginia Tech Center of Excellence in Emerging Materials, Thapar Institute of Engineering and Technology, Patiala 147004, India;* ⊙ orcid.org/0000-0003-0286-9028; Email: banibrata.maity@thapar.edu

Author

Aayushi Kundu − *School of Chemistry and Biochemistry, Senior Research Fellow—TIET-Virginia Tech Center of Excellence in Emerging Materials, Thapar Institute of Engineering and Technology, Patiala 147004, India*

Complete contact information is available at:
https://pubs.acs.org/10.1021/acsomega.3c05424

Notes

The authors declare no competing financial interest.

REFERENCES

(1) Sudha, P. N.; Sangeetha, K.; Vijayalakshmi, K.; Barhoum, A. Nanomaterials History, Classification, Unique Properties, Production and Market. In *Emerging applications of nanoparticles and architecture nanostructures*; Elsevier, 2018; pp 341−384.

(2) Sohal, N.; Maity, B.; Basu, S. Morphology-Dependent Performance of MnO2 Nanostructure-Carbon Dot-Based Biosensors for the Detection of Glutathione. *ACS Appl. Bio Mater.* **2021**, *4* (6), 5158−5168.

(3) Kundu, A.; Maity, B.; Basu, S. Rice Husk-Derived Carbon Quantum Dots-Based Dual-Mode nanoprobe for Selective and Sensitive Detection of Fe3+ and Fluoroquinolones. *ACS Biomater. Sci. Eng.* **2022**, *8*, 4764.

(4) Khan, Z. M. S. H.; Rahman, R. S.; Shumaila; Islam, S.; Zulfequar, M. Hydrothermal Treatment of Red Lentils for the Synthesis of Fluorescent Carbon Quantum Dots and Its Application for Sensing Fe3+. *Opt. Mater. (Amst.)* **2019**, *91*, 386−395.

(5) Atchudan, R.; Edison, T. N. J. I.; Aseer, K. R.; Perumal, S.; Karthik, N.; Lee, Y. R. Highly Fluorescent Nitrogen-Doped Carbon Dots

Derived from Phyllanthus Acidus Utilized as a Fluorescent Probe for Label-Free Selective Detection of Fe3+ Ions, Live Cell Imaging and Fluorescent Ink. *Biosens. Bioelectron.* **2018**, *99*, 303−311.

(6) Jones, S. S.; Sahatiya, P.; Badhulika, S. One Step, High Yield Synthesis of Amphiphilic Carbon Quantum Dots Derived from Chia Seeds: A Solvatochromic Study. *New J. Chem.* **2017**, *41* (21), 13130−13139.

(7) Chatzimitakos, T.; Kasouni, A.; Sygellou, L.; Avgeropoulos, A.; Troganis, A.; Stalikas, C. Two of a Kind but Different: Luminescent Carbon Quantum Dots from Citrus Peels for Iron and Tartrazine Sensing and Cell Imaging. *Talanta* **2017**, *175*, 305−312.

(8) Tyagi, A.; Tripathi, K. M.; Singh, N.; Choudhary, S.; Gupta, R. K. Green Synthesis of Carbon Quantum Dots from Lemon Peel Waste: Applications in Sensing and Photocatalysis. *RSC Adv.* **2016**, *6* (76), 72423−72432.

(9) Su, A.; Wang, D.; Shu, X.; Zhong, Q.; Chen, Y.; Liu, J.; Wang, Y. Synthesis of Fluorescent Carbon Quantum Dots from Dried Lemon Peel for Determination of Carmine in Drinks. *Chem. Res. Chin. Univ.* **2018**, *34* (2), 164−168.

(10) Qi, H.; Huang, D.; Jing, J.; Ran, M.; Jing, T.; Zhao, M.; Zhang, C.; Sun, X.; Sami, R.; Benajiba, N. Transforming Waste into Value: Pomelo-Peel-Based Nitrogen-Doped Carbon Dots for the Highly Selective Detection of Tetracycline. *RSC Adv.* **2022**, *12* (12), 7574−7583.

(11) Wang, C.; Sun, Q.; Yang, M.; Liu, E.; Xue, W.; Fan, J. Preparation of Highly Luminescent Nitrogen-Doped Carbon Quantum Dots and Their Detection of Tetracycline Antibiotics. *Colloids Surf., A* **2022**, *653*, No. 129982.

(12) Zhao, W.; Zuo, H.; Guo, Y.; Liu, K.; Wang, S.; He, L.; Jiang, X.; Xiang, G.; Zhang, S. Porous Covalent Triazine-Terphenyl Polymer as Hydrophilic−Lipophilic Balanced Sorbent for Solid Phase Extraction of Tetracyclines in Animal Derived Foods. *Talanta* **2019**, *201*, 426−432.

(13) Wang, G.; Zhang, H. C.; Liu, J.; Wang, J. P. A Receptor-Based Chemiluminescence Enzyme Linked Immunosorbent Assay for Determination of Tetracyclines in Milk. *Anal. Biochem.* **2019**, *564*, 40−46.

(14) Mu, G.; Liu, H.; Xu, L.; Tian, L.; Luan, F. Matrix Solid-Phase Dispersion Extraction and Capillary Electrophoresis Determination of Tetracycline Residues in Milk. *Food Anal. Methods* **2012**, *5*, 148−153.

(15) Sattayasamitsathit, S.; Thavarungkul, P.; Kanatharana, P. Bismuth Film Electrode for Analysis of Tetracycline in Flow Injection System. *Electroanal.: Int. J. Fundam. Pract. Aspects Electroanal.* **2007**, *19* (4), 502−505.

(16) Charoenraks, T.; Chuanuwatanakul, S.; Honda, K.; Yamaguchi, Y.; Chailapakul, O. Analysis of Tetracycline Antibiotics Using HPLC with Pulsed Amperometric Detection. *Anal. Sci.* **2005**, *21* (3), 241−245.

(17) Kundu, A.; Maity, B.; Basu, S. Coal-Derived Graphene Quantum Dots with a Mn2+/Mn7+ nanosensor for Selective Detection of Glutathione by a Fluorescence Switch-off-on Assay. *New J. Chem.* **2022**, *46* (16), 7545−7556.

(18) Sohal, N.; Bhatia, S. K.; Basu, S.; Maity, B. nanomolar Level Detection of Metal Ions by Improving the monodispersity and Stability of Nitrogen-Doped Graphene Quantum Dots. *New J. Chem.* **2021**, *45* (42), 19941−19949.

(19) Liu, M. L.; Chen, B.; Bin; Yang, T.; Wang, J.; Liu, X. D.; Huang, C. Z. One-Pot Carbonization Synthesis of Europium-Doped Carbon Quantum Dots for Highly Selective Detection of Tetracycline. *Methods Appl. Fluoresc.* **2017**, *5* (1), No. 015003, DOI: 10.1088/2050-6120/aa5e2b.

(20) Fan, Y.; Qiao, W.; Long, W.; Chen, H.; Fu, H.; Zhou, C.; She, Y. Detection of Tetracycline Antibiotics Using Fluorescent "Turn-off" Sensor Based on S, N-Doped Carbon Quantum Dots. *Spectrochim. Acta, Part A* **2022**, *274*, No. 121033.

(21) Qi, H.; Teng, M.; Liu, M.; Liu, S.; Li, J.; Yu, H.; Teng, C.; Huang, Z.; Liu, H.; Shao, Q.; Umar, A.; Ding, T.; Gao, Q.; Guo, Z. Biomass-Derived Nitrogen-Doped Carbon Quantum Dots: Highly Selective Fluorescent Probe for Detecting Fe 3+ Ions and Tetracyclines. *J. Colloid Interface Sci.* **2019**, *539*, 332−341.

(22) Zhang, Z.; Fan, Z. Application of Cerium−Nitrogen Co-Doped Carbon Quantum Dots to the Detection of Tetracyclines Residues and Bioimaging. *Microchem. J.* **2021**, *165*, No. 106139.

(23) John, B. K.; John, N.; Korah, B. K.; Thara, C.; Abraham, T.; Mathew, B. Nitrogen-Doped Carbon Quantum Dots as a Highly Selective Fluorescent and Electrochemical Sensor for Tetracycline. *J. Photochem. Photobiol., A* **2022**, *432*, No. 114060.

(24) Demasa, J. N.; Crosby, G. A. The Measurement of Photoluminescence Quantum Yields. 1 A Review2. *J. Chem. Phys.* **1968**, *48*, 4726.

(25) Atchudan, R.; Edison, T. N. J. I.; Perumal, S.; Lee, Y. R. Green Synthesis of Nitrogen-Doped Graphitic Carbon Sheets with Use of Prunus Persica for Supercapacitor Applications. *Appl. Surf. Sci.* **2017**, *393*, 276−286.

(26) Wang, J.; An, J.; Zhang, Z.; Zhu, H.; Liang, X.; Yang, S.; Sheng, K.; Chen, L.; Lu, H.; Wang, Y. High Fluorescent Nitrogen− Doped Carbon Dots Derived from Sanghuangporus Lonicericola for Detecting Tetracyclines in Aquaculture Water and Rat Serum Samples. *Microchem. J.* **2023**, *189*, No. 108517.

(27) Singh, V. K.; Singh, V.; Yadav, P. K.; Chandra, S.; Bano, D.; Kumar, V.; Koch, B.; Talat, M.; Hasan, S. H. Bright-Blue-Emission Nitrogen and Phosphorus-Doped Carbon Quantum Dots as a Promising nanoprobe for Detection of Cr(vi) and Ascorbic Acid in Pure Aqueous Solution and in Living Cells. *New J. Chem.* **2018**, *42* (15), 12990−12997.

(28) Kundu, A.; Maity, B.; Basu, S. Orange Pomace-Derived Fluorescent Carbon Quantum Dots: Detection of Dual Analytes in the nanomolar Range. *ACS Omega* **2023**, *8* (24), 22178−22189.

(29) Yang, F.; Bao, W.; Liu, T.; Zhang, B.; Huang, S.; Yang, W.; Li, Y.; Li, N.; Wang, C.; Pan, C.; Li, Y. Nitrogen-Doped Graphene Quantum Dots Prepared by Electrolysis of Nitrogen-Doped Nanomesh Graphene for the Fluorometric Determination of Ferric Ions. *Microchim. Acta* **2020**, *187* (6), 1−10, DOI: 10.1007/s00604-020-04294-8.

(30) Wang, C.; Pan, C.; Wei, Z.; Liu, J.; Song, Z.; Ma, W.; Wang, M.; Mao, L. One-Step Synthesis of Nitrogen-Doped Multi-Emission Carbon Dots and Their Fluorescent Sensing in HClO and Cellular Imaging. *Microchim. Acta* **2021**, *188*, 1−11, DOI: 10.1007/s00604-021-04973-0.

(31) Liang, Y.-M.; Yang, H.; Zhou, B.; Chen, Y.; Yang, M.; Wei, K.-S.; Yan, X.-F.; Kang, C. Waste Tobacco Leaves Derived Carbon Dots for Tetracycline Detection: Improving Quantitative Accuracy with the Aid of Chemometric Model. *Anal. Chim. Acta* **2022**, *1191*, No. 339269.

(32) Ding, H.; Yu, S. B.; Wei, J. S.; Xiong, H. M. Full-Color Light-Emitting Carbon Dots with a Surface-State-Controlled Luminescence Mechanism. *ACS Nano* **2016**, *10* (1), 484−491.

(33) Gan, Z.; Xu, H.; Hao, Y. Mechanism for Excitation-Dependent Photoluminescence from Graphene Quantum Dots and Other Graphene Oxide Derivates: Consensus, Debates and Challenges. *Nanoscale* **2016**, *8* (15), 7794−7807.

(34) Kurniawan, D.; Chiang, W.-H. Microplasma-Enabled Colloidal Nitrogen-Doped Graphene Quantum Dots for Broad-Range Fluorescent PH Sensors. *Carbon* **2020**, *167*, 675−684.

(35) Zhang, J.; Na, L.; Jiang, Y.; Lou, D.; Jin, L. Graphene Quantum Dots as a Fluorescence-Quenching Probe for Quantitative Analysis of Ponceau 4R Solution. *Anal. Methods* **2016**, *8* (39), 7242−7246.

(36) Li, C.; Yue, Y. Fluorescence Spectroscopy of Graphene Quantum Dots: Temperature Effect at Different Excitation Wavelengths. *Nanotechnology* **2014**, *25* (43), No. 435703.

(37) Guideline, I. C. H. H. T. Validation of Analytical Procedures: Text and Methodology. *Q2(R1)* **2005**, *1* (20), 5.

(38) Lakowicz, J. R. *Principles of Fluorescence Spectroscopy*; Springer, 2006. DOI: 10.1007/978-0-387-46312-4.

(39) Yan, Y.; Liu, J. H.; Li, R. S.; Li, Y. F.; Huang, C. Z.; Zhen, S. J. Carbon Dots Synthesized at Room Temperature for Detection of Tetracycline Hydrochloride. *Anal. Chim. Acta* **2019**, *1063*, 144−151.

(40) Zhou, R.; Chen, C.; Hu, J.; Liao, X.; Hu, H.; Tong, Z.; Liang, J.; Huang, F. The Self-Nitrogen-Doped Carbon Quantum Dots Derived from Morus Alba L. Leaves for the Rapid Determination of Tetracycline. *Ind. Crops Prod.* **2022**, *188*, No. 115705.

(41) Wei, X.; Lv, L.; Zhang, Z.; Guan, W. Preparation of Molecularly Imprinted Fluorescence Sensor Based on Carbon Quantum Dots via Precipitation Polymerization for Fluorescence Detection of Tetracycline. *J. Appl. Polym. Sci.* **2020**, *137* (38), 49126 DOI: 10.1002/app.49126.

(42) Yang, Y.; Liu, Z.; Chen, D.; Gu, B.; Gao, B.; Wang, Z.; Guo, Q.; Wang, G. Multifunctional N-Doped Graphene Quantum Dots towards Tetracycline Detection, Temperature Sensing and High-Performance WLEDs. *J. Photochem. Photobiol., A* **2021**, *405*, No. 112977.

(43) Xing, X.; Huang, L.; Zhao, S.; Xiao, J.; Lan, M. S, N-Doped Carbon Dots for Tetracyclines Sensing with a Fluorometric Spectral Response. *Microchem. J.* **2020**, *157*, No. 105065.

(44) Shi, W.; Guo, F.; Han, M.; Yuan, S.; Guan, W.; Li, H.; Huang, H.; Liu, Y.; Kang, Z. N, S Co-Doped Carbon Dots as a Stable Bio-Imaging Probe for Detection of Intracellular Temperature and Tetracycline. *J. Mater. Chem. B* **2017**, *5* (18), 3293−3299.

(45) Deng, X.; Feng, Y.; Li, H.; Du, Z.; Teng, Q.; Wang, H. N-Doped Carbon Quantum Dots as Fluorescent Probes for Highly Selective and Sensitive Detection of Fe3+ Ions. *Particuology* **2018**, *41*, 94−100.

(46) Zu, F.; Yan, F.; Bai, Z.; Xu, J.; Wang, Y.; Huang, Y.; Zhou, X. The Quenching of the Fluorescence of Carbon Dots: A Review on Mechanisms and Applications. *Microchim. Acta* **2017**, *184* (7), 1899−1914.

(47) Lin, M.; Zou, H. Y.; Yang, T.; Liu, Z. X.; Liu, H.; Huang, C. Z. An Inner Filter Effect Based Sensor of Tetracycline Hydrochloride as Developed by Loading Photoluminescent Carbon Nanodots in the Electrospun Nanofibers. *Nanoscale* **2016**, *8* (5), 2999−3007.

(48) Zhao, C.; Jiao, Y.; Gao, Z.; Yang, Y.; Li, H. N, S Co-Doped Carbon Dots for Temperature Probe and the Detection of Tetracycline Based on the Inner Filter Effect. *J. Photochem. Photobiol., A* **2018**, *367*, 137−144.

(49) Han, L.; Fan, Y. Z.; Qing, M.; Liu, S. G.; Yang, Y. Z.; Li, N. B.; Luo, H. Q. Smartphones and Test Paper-Assisted Ratiometric Fluorescent Sensors for Semi-Quantitative and Visual Assay of Tetracycline Based on the Target-Induced Synergistic Effect of Antenna Effect and Inner Filter Effect. *ACS Appl. Mater. Interfaces* **2020**, *12* (41), 47099−47107.

(50) Zhang, L.; Wang, Y.; Jia, L.; Bi, N.; Bie, H.; Chen, X.; Zhang, C.; Xu, J. Ultrasensitive and Visual Detection of Tetracycline Based on Dual-Recognition Units Constructed Multicolor Fluorescent Nano-Probe. *J. Hazard. Mater.* **2021**, *409*, No. 124935.